JOURNAL OF APPLIED ELECTROCHEMISTRY 23 (1993) 606–614

Investigations of nonlinear processes by transients: kinetics of dissolution of inhibitor layers on copper*

M. BEIER, M. M. LOHRENGEL, J. W. SCHULTZE

Institut für Physikalische Chemie und Elektrochemie, Heinrich-Heine-Universität Düsseldorf, D-4000 Düsseldorf 1, Germany

Received 14 July 1992; revised 2 November 1992

The dissolution of inhibitor layers of AHT (3-amino-5-heptyl-1,2,4-triazole) on copper wires in 0.5 M H_2SO_4 was studied by potentiostatic current and capacity transients in a time range from 10 μs to 1000 s. The potential dependent transients show three characteristic regions corresponding to different transfer controlled processes. For short periods an almost constant current of inhibited corrosion through a metastable inhibitor layer is observed. In the second region the dissolution of this layer causes a strong increase in copper corrosion, which was taken as a direct measure of the desorption process. The electrode capacity, C, increases correspondingly. The dissolution itself is not accompanied by a notable charge transfer and, hence, cannot directly be monitored. The last region is dominated by an almost constant active copper dissolution current. The layer dissolution in the second region starts with an inhomogeneous nucleation process. Initially, holes are generated stochastically in the AHT layer and form nuclei of corrosion pits on the copper surface. Based on this model the complete transients can be calculated.

Notation

b_{free}	Tafel slope of an uncovered copper electrode
b_{nucl}	potential dependence of pit formation (Equation 23)
b_3	$b_3 = dU/d \log (di_{pits}/dt^3)$
C	electrode capacity
D	dielectric constant of the layer
D_0	dielectric constant of the vacuum
d	layer thickness
F	Faraday constant
I_1	time dependent corrosion current of a single pit
i	total current density
i_{free}	corrosion current density of an uncovered copper electrode
i_{inh}	current density of an inhibited copper electrode
i_{pits}	corrosion current density of n pits
i_{0V}	extrapolated value of I_{free} at 0 V vs SHE
n	time dependent number of pits
n_{max}	maximum number of pits
r	time dependent radius of a single pit
S	total area of all pits
t	time
U	potential against SHE
U_{nucl}	potential of hole formation
V	molar volume
z	charge number
θ	degree of coverage of inhibitor

1 Introduction

Normally, adsorption and desorption organic molecules are investigated under equilibrium, steady state or quasisteady conditions, e.g. [1]. Stimulating ideas on methods and problems have been contributed by Conway [2]. For technically relevant corrosion inhibitors, however, a knowledge about the kinetics is very small and the reasons for this are simple. Detailed studies of the inhibition mechanism are difficult. The inhibition process is a complex combination of corrosion, precipitation, irreversible coadsorption of the components, nucleation, and layer ageing. The systems do not reach a real steady state. The nature of the inhibition process and the corrosion in parallel cause difficulties with the reproducibility of experiments. Therefore, it has been necessary to develop a multipulse program to produce defined surface conditions as discussed by Gilman [3] and Trasatti [4] for problems of electrocatalysis. Potentiodynamic investigations concerning the adsorption and desorption of organic molecules accompanied by corrosion have been carried out by Drazic [5].

After the successful application of potentiostatic pulse techniques to other nonlinear, time-dependent processes [6] investigations of the formation [7, 8] and dissolution of inhibitor layers have been carried out.

3-Amino-5-heptyl-1,2,4-triazole (AHT) is a com-

*This paper is dedicated to Professor Brian E. Conway on the occasion of his 65th birthday, and in recognition of his outstanding contribution to electrochemistry.

0021-891X/93

mercially applied [9] effective inhibitor of the corrosion of copper, zinc, brass and other copper alloys in neutral or acid aqueous solutions. It is used in closed cold and hot water systems. Commercially available is the hydrochloride of AHT, which is sufficiently soluble in water. AHT was chosen, since this inhibitor is effective in acid solutions, where side reactions, e.g.copper oxide formation, can be avoided. Furthermore, AHT may be removed easily at higher potential.

Under potentiostatic conditions, the current density, i, of many time-dependent processes are well described by the 'universal law'.

$$i \propto t^m \tag{1}$$

In a double logarithmic representation, $\log i$ against $\log t$, the power of t can be derived from the slope, m:

$$\frac{\mathrm{d}\log(i)}{\mathrm{d}\log(t)} = m \tag{2}$$

Typical values of m have been summarized in a previous paper [10].

An experimental verification of this law requires measurements over some orders of magnitude of current and time. An extension to short times ($\ll 1$ s) is preferable to avoid processes of ageing and reorganization. In this case sophisticated equipment is necessary [6, 11], especially when the investigations are extended to very short times of the order of microseconds.

2. Experimental details

2.1. *Electrodes, solutions, and electronic equipment*

The experiments were carried out in a Pyrex glass cell at 25° C. The working electrodes consisted of spectroscopically pure copper wires (99.999%, Johnson Matthey GmbH) with a diameter of 0.5 mm. Immediately before the measurements the electrodes were electropolished anodically in 75% H_3PO_4 phosphoric acid at 0.2 A cm^{-2}. The wires were dipped 1.5 cm into the solution (vol. 40 ml) so that the effective surface was 0.23 cm^2. The uncompensated electrolyte resistance is about $R_{el} = 0.25\,\Omega\,\mathrm{cm}^2$ and was determined by EIS [12]. For each measurement a new electrode was used.

All potentials are referred to the standard hydrogen electrode (SHE). The purity of the inhibitor 3-amino-5-heptyl-1,2,4-triazole with HCl (AHT·HCl, Henkel KGaA, Düsseldorf, with Trademark Texamin AT 1) was >95%. The measurements were carried out in an aqueous and aerated solution of 0.5 M H_2SO_4 at an inhibitor concentration of $c_{inh} = 2 \times 10^{-3}$ M. For the preparation of the solutions only p.a. chemicals and deionized water (Millipore) were used.

The potential was controlled by a fast rise potentiostat. The current was measured using an autoranging differential amplifier. Both devices are in-house developments. The current signal was digitized by a Krenz transient recorder TRM 4000 and processed by a DEC LSI 11/23 computer. The transients were recorded with a resolution in time of 1 μs in the beginning, decreasing with time. Typically, 100 samples per time decade were taken for a detailed kinetic investigation. The capacity of the electrode surface was measured by a special pulse technique. This technique [13, 14] has a high resolution in time ($\ll 1$ ms) and is applicable to nonsteady systems as long as Faradaic current densities are small, $i_{Far} < 10\,\mathrm{mA\,cm}^{-2}$.

2.2. *Potential time program for layer desorption*

To study the layer desorption process it is necessary to obtain exactly reproducible conditions before measurements can take place. The adsorption layers of AHT tend to change their properties irreproducibly with time due to reorganisation, ageing, and precipitation effects. The conditions under which the electrode is immersed in the electrolyte cannot be controlled exactly. Therefore, a special pretreatment in the electrolyte is necessary. With respect to this, a special time pulse program was developed to obtain well defined layers (Fig. 1).

After immersing the electrode in the electrolyte an initial potential of 0.35 V was applied for 300 s. Under these conditions the surface is covered by AHT. Then, the potential was stepped to the potential $U_{clean} = 0.5$ V for 10 s to remove most of the layer of AHT to obtain a reproducible free surface [8]. The potential was stepped down to form an adsorption layer at $U_{ad} = 0.35$ V for 50 s. This treatment leads to an exactly defined AHT-layer. Finally the potential was stepped to the desorption potential, U, to dissolve the layer again. The corresponding current transient $i(t)$ was recorded simultaneously and the desorption process was examined.

3. Desorption transients

Since the electrosorption valency of AHT is presumably very small, the desorption or adsorption of AHT is not accompanied by charge transfer. However, this process can be followed indirectly by capacity measurements or by measurements of the corrosion current of the uncovered parts of the electrode. In both cases, a significant difference of properties between the covered and uncovered parts is necessary.

The dependence of current density on time at var-

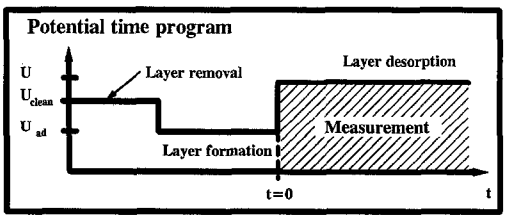

Fig. 1. Potential time program for the measurement of desorption of well defined AHT layers. First desorption to get a clean surface by copper corrosion at $U_{clean} = 0.5$ V, $t_{clean} = 10$ s, defined layer formation at $U_{ad} = 0.35$ V during $t_{ad} = 50$ s, final measurement of dissolution transient at U.

ious desorption potentials, U, is shown in a double logarithmic plot, Fig. 2. At low potentials, i.e. < 400 mV, no desorption is observed. The current is dominated by a quasistationary 'passive' corrosion of the AHT covered metal. This current decreases slightly with time, indicating the better protection effect of aged layers. In the mean potential range (most pronounced from 480 to 650 mV) the transients can be separated into three regions. In the first region a constant current through the metastable AHT layer is observed, depending on the potential. The second region is characterized by a strong increase in corrosion. This indicates dissolution of the protecting layer. Finally, an almost constant current of active copper dissolution ($i > 100\,\mathrm{mA\,cm^{-2}}$, controlled by R_{el}) is found in the last region. The second region shifts with increasing potential to shorter times. At potentials $U > 650$ mV the currents are high, even at the beginning, and an adequate potential control becomes impossible because of the uncompensated part of the electrolyte resistance. This explains the smaller slope at higher potentials (700 mV).

It is possible to explain the dissolution of the inhibitor layer by only one potential dependent mechanism. In principle, either a homogeneous or an inhomogeneous removal of the layer may be assumed.

In the first case, a homogeneous decrease of the inhibitor layer thickness, d, is supposed. The corrosion current should depend on the layer thickness. This dependence is determined by the transport mechanism of the corrosion products through the layer. When the transport is a field-dependent migration, the corrosion current is given by:

$$i \propto \exp\left(\frac{A}{d}\right) \tag{3}$$

When the transport is diffusion controlled (less probable), the current is

$$i \propto \frac{\mathrm{d}c}{\mathrm{d}d} \propto \frac{1}{d} \tag{4}$$

In both cases, the electrode capacity, C, is given by the capacitor equation:

$$C = \frac{DD_0}{d} \propto \frac{1}{d} \tag{5}$$

Hence, the dependence of i on C should be linear for a diffusion controlled process only and a distinction of migration and diffusion is possible. The deviations from linearity for migration, however, may be small when the thickness d does not change over a wider range.

In the second case the inhomogeneous dissolution causes free parts of the electrode while others are covered with an almost unchanged layer. The total current, i, depends on the degree of coverage θ of inhibitor:

$$i = (1 - \theta) i_{\mathrm{free}} + \theta i_{\mathrm{inh}} \tag{6}$$

i_{free} or i_{inh} are the corrosion current densities of the free and covered parts of the electrode. The electrode capacity, C, shows a similar dependence:

$$C = (1 - \theta) C_{\mathrm{free}} + \theta C_{\mathrm{inh}} \tag{7}$$

Therefore, a plot of i against C is also linear. Actually, a linear dependence is found as illustrated in Fig. 3 and, together with the following evaluation, it can be demonstrated that an inhomogeneous model describes the dissolution correctly.

The evolution of the uncovered parts can be described in terms of a germ nucleation process. Holes in the inhibitor layer are formed stochastically

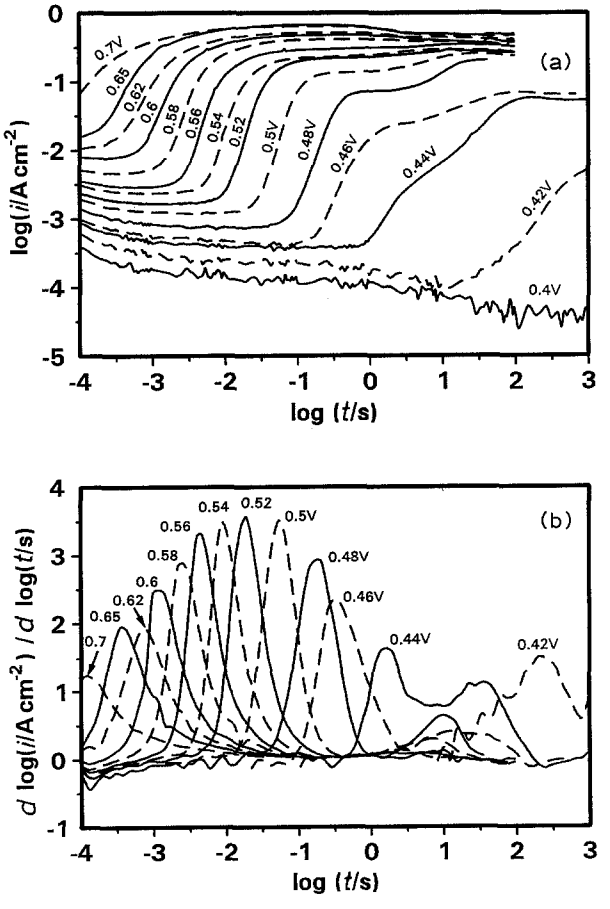

Fig. 2. (a) Current densities of potentiostatic AHT layer dissolution in a double logarithmic plot at various U in 0.5 M H_2SO_4 with $c_{\mathrm{inh}} = 2 \times 10^{-3}$ M and $T = 298$ K. (b) First derivatives of the current densities of (a).

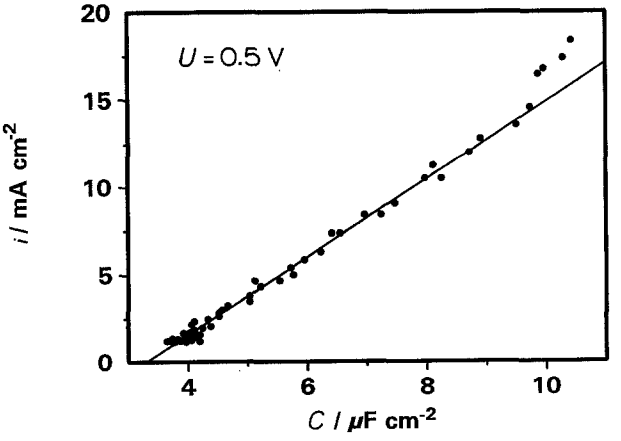

Fig. 3. Current of a transient at $U = 0.5$ V against the electrode capacity. $C = 10\,\mu\mathrm{F\,cm^{-2}}$ are reached after 700 μs.

with time. When the area of a hole exceeds a critical value (critical nucleus), it is able to grow on, Fig. 4. At the bottom of a hole the electrode surface starts to corrode and hemispherical pits are formed. The total number and the individual diameters, d, of the pits increase with time, t. Hence, the total current density also increases due to the strong corrosion of the uncovered parts. The formation rate of holes may depend on time and potential.

In the lower part of Fig. 2 the first derivative of the current transients is given. In the central part the slope is close to 3:

$$\frac{\mathrm{d}\log(i)}{\mathrm{d}\log(t)} = 3 \tag{8}$$

This means a time dependence of current:

$$i \propto t^3 \tag{9}$$

or

$$i = a + bt^3 \tag{10}$$

where a is the potential dependent corrosion current through the metastable 'passive' layer of AHT. a is equal to θi_{ihn}, corresponding to Equation 6. With increasing values of t, Equation 10 approaches Equation 9, if

$$a \ll bt^3 \tag{11}$$

A better test is a plot of i against t^3, corresponding to Equation 10. The values of i and t depend on the potential and change over wide range of more than four decades. Hence, it is better to normalize their values. Therefore, i/i_{infl} is plotted against $(t/t_{\mathrm{infl}})^3$ (Fig. 5), where i_{infl} and t_{infl} are the currents and times of the point of inflection of the corresponding transient. Values for t_{infl} and i_{infl} were taken from the maxima of the derivatives (Fig. 2(b), t_{infl}) and the corresponding currents from Fig. 2(a).

The data at different potentials are linear, as expected. From the axis intercept the corrosion current through the inhibitor layer can be calculated (Equation 10), but more precise values are taken directly from the transients (Fig. 2).

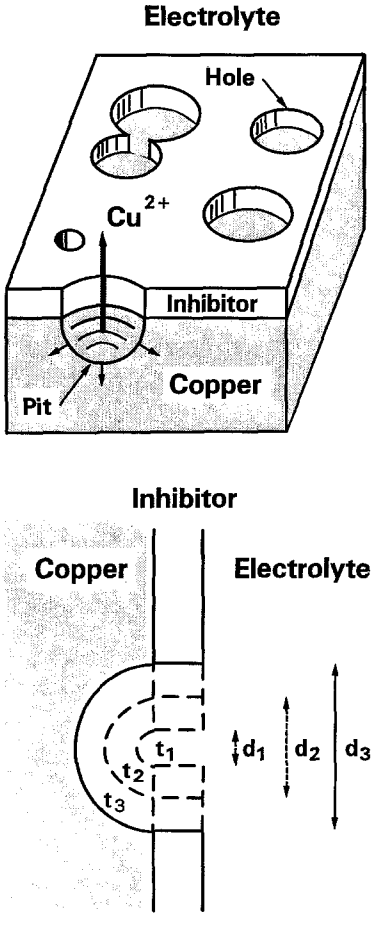

Fig. 4. (a) Schematic representation of the interface showing some holes in the layer and an underlying pit in the metal phase. (b) Pit growth for different diameters d and times t.

4. Model

A detailed model of the AHT dissolution process is presented in the following Section. Similar models for electrodeposition were developed by Avrami [15] and for pitting corrosion of passivated iron in the absence of inhibitors by Strehblow [16] and Engell [17]. A definitive proof for this model comes from some additional experiments, which show results predicted by the model (Section 4.3).

4.1. *Base model*

When a hole exceeds the size of a critical nucleus, it continues to grow. The corrosion current density in the growing pit may be equal to the corrosion current density, i_{free}, of the active copper. The potential dependence of this current is approximated by:

$$i_{\mathrm{free}} = i_{0\mathrm{v}} \exp\left(\frac{U}{0.4343 b_{\mathrm{free}}}\right) \tag{12}$$

This equation is not referred to the equilibrium potential of copper, but to 0 V vs SHE due to the undefined copper concentration. Therefore, $i_{0\mathrm{V}}$ is not an exchange current density.

A homogeneous dissolution forms hemispherical pits. The current, I_1, of a single pit depends on its

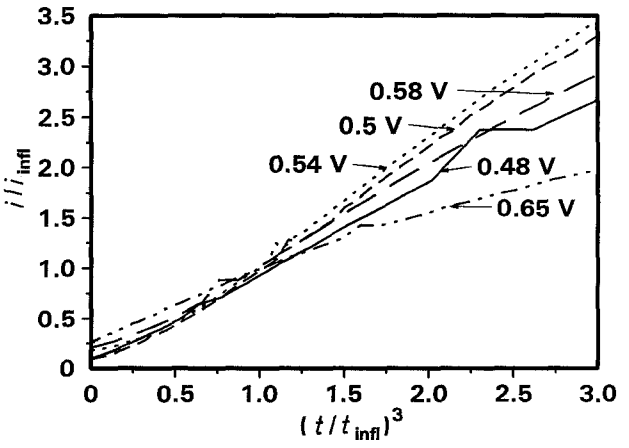

Fig. 5. Normalized current densities i/i_{infl} in dependence on the normalized time $(t/t_{\mathrm{infl}})^3$ for various values of U. The reference values t_{infl} are taken from the maxima of the derivatives in Fig. 2(b). The corresponding values of i_{infl} are taken from Fig. 2(a).

radius, r:

$$I_1 = i_{free} 2\pi r^2 \tag{13}$$

The increase of r with time is given by the corrosion current and Faraday's law:

$$\frac{dr}{dt} = \frac{V}{zF} i_{free} \tag{14}$$

where V is the molar volume of copper and z the charge number. The radius of a pit of age t_a is:

$$r = \frac{V i_{free}}{zF} \int_0^{t_a} dt = \frac{V i_{free}}{zF} t_a \tag{15}$$

and the current I_1 in a single pit:

$$I_1 = 2\pi i_{free}^3 \left(\frac{V}{zF}\right)^2 t_a^2 \tag{16}$$

The current density $i_{pits} = (1-\theta) i_{free}$ of all pits can be calculated from the number, n, of pits per cm^2:

$$I_{pits} = n I_1 = 2\pi n i_{free}^3 \left(\frac{V}{zF}\right)^2 t_a^2 \tag{17}$$

This equation is true when all nuclei are formed at the beginning of the transient. In this case the current density is proportional to t^2. The experimental current transients, however, are proportional to t^3. Hence, a progressive nucleation of the pits must be assumed. There are two fundamental concepts: the maximum number of pits which could be formed is infinite (indexed equation 'a') or limited by n_{max} (equation 'b').

The time dependent number of pits is given by:

$$n(t) = n_0 k t \tag{18 a}$$

$$n(t) = n_{max}(1 - \exp(-kt)) \tag{18 b}$$

and the corresponding formation rates:

$$\frac{dn}{dt} = n_0 k \tag{19 a}$$

$$\frac{dn}{dt} = n_{max} k \exp(-kt) \tag{19 b}$$

Different pits may have different ages t_a and, hence, different radii. This distribution of age has to be considered. When the system is observed at a random moment t, there are dn_a pits with an age of t_a. These were formed at the moment $t - t_a$ with a corresponding formation rate, which can be taken from Equation 19:

$$dn_a = n_0 k \, dt_a \tag{20 a}$$

$$dn_a = n_{max} k \exp(-k(t - t_a)) \, dt_a \tag{20 b}$$

The part di_{pits} of the total current density, which is caused by these pits with an age t_a is given by [16]:

$$di_{pits} = I_1 \, dn_a \tag{21}$$

and the total current density i_{pits} by:

$$i_{pits} = 2\pi n_0 k i_{free}^3 \left(\frac{V}{zF}\right)^2 \int_0^t t_a^2 \, dt_a = \tfrac{2}{3}\pi n_0 k i_{free}^3 \left(\frac{V}{zF}\right)^2 t^3 \tag{22 a}$$

$$i_{pits} = 2\pi n_{max} k i_{free}^3 \left(\frac{V}{zF}\right)^2 \exp(-kt) \int_0^t t_a^2 \exp(kt_a) \, dt_a \tag{22 b}$$

$$= 2\pi n_{max} i_{free}^3 \left(\frac{V}{zF}\right)^2 \left(t^2 - \frac{2t}{k} + \frac{2 - 2\exp(-kt)}{k^2}\right)$$

Equation 22(a) shows the expected t^3-dependence as well as Equation 22(b) for shorter periods. For longer periods of time the formation of pits in Equation 22(b) decreases and the dependence changes to t^2.

The current i_{pits} in Equation 22(a) and (b) is equal to $(1-\theta) i_{free}$ in Equation 6 and refers to that part of the surface which is free of inhibitor. The corrosion current of the covered part has to be added (Equation 10). This current is almost constant initially ($\theta \approx 1$) and can be neglected later, because of the much higher active corrosion of the uncovered metal. Hence, a constant value as shown in Equation 10 is sufficient.

The correspondence of model and experiment is good (cf. Section 4.2), but no final proof is established. A further confirmation comes from an explanation of the potential dependence and some additional pulse experiments (Section 4.3). The potential dependence of the pit formation rate k has been described by a decrease of the activation energy by the potential:

$$n_0 k = n' \exp\left(\frac{U - U_{nucl}}{0.4343 b_{nucl}}\right) \tag{23}$$

where $U - U_{nucl}$ is an overpotential of pit formation. Substituting $n_0 k$ into Equation 22(a), the current i_{pits} increases exponentially with the overpotential:

$$i_{pits} = \tfrac{2}{3}\pi n' i_{free}^3 \left(\frac{V}{zF}\right)^2 \exp\left(\frac{U - U_{nucl}}{b_{nucl} 0.4343}\right) t^3 \tag{24}$$

Equation 24 can be linearized using Equation 12:

$$\log\left(\frac{di_{pits}}{dt^3}\right) = \frac{U - U_{nucl}}{b_{nucl}} + \log\left(\frac{2}{3}\pi n' i_{free}^3 \left(\frac{V}{zF}\right)^2\right)$$

$$= \left(\frac{1}{b_{nucl}} + \frac{3}{b_{free}}\right) U - \frac{U_{nucl}}{b_{nucl}}$$

$$+ \log\left(\frac{2}{3}\pi n' i_{0V}^3 \left(\frac{V}{zF}\right)^2\right) \tag{25}$$

The corresponding potential dependence is given in Fig. 6. The linearity is sufficient for potentials from 500 to 700 mV. The nucleation of pits seems to be a random, potential supported process. The corresponding linearization of Equation 22(b) is impossible.

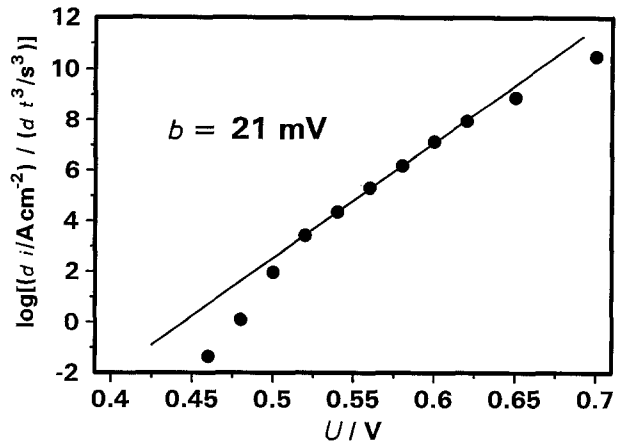

Fig. 6. Logarithmic plot of the slopes di/dt^3 against the potential U.

4.2. *Calculations and simulations*

The available set of equations and data is sufficient to calculate complete current transients. The computations are based on Equation 6:

$$i = i_{\text{pits}} + \theta i_{\text{inh}} \approx i_{\text{pits}} + i_{\text{inh}} \tag{26}$$

Equation 24 is used to substitute i_{pits}. When the sum of the areas of all pits exceeded 1 cm^2, which is the total area of the normalized surface, the current i was restricted to a constant value.

It is not easy to obtain reliable numerical data for the potential dependence of i_{free} and i_{inh}. Values of the free corrosion (i_{free}) are already published (e.g. [18]), but depend on the electrolyte, on the surface activity, and, especially for higher currents, on the limitations of the potentiostatic equipment. Hence, the corrosion current of the free surface in the electrolyte has been measured (compare [8]). The Tafel plot corresponding to Equation 12 is presented in Fig. 7 and linearized to

$$\log(i_{\text{free}}) = \frac{U}{76\,\text{mV}} - 7.17 \tag{27}$$

which is the best fit in the range 300 mV < U < 400 mV.

These values correspond to measurements of a large area in the present electrolyte. The growing pits, however, are embedded in a different neighbourhood (small hemispherical pits surrounded by inhibitor layer) and behave like microelectrodes. Nevertheless, these data were taken as a sufficient approximation.

The AHT layer is not stable for potentials exceeding 400 mV and, therefore, it is impossible to measure a steady value of i_{inh}. At the beginning of the transients (Fig. 2) i_{inh} is observed as long as the layer is metastable. Figure 8 shows the current minima in the form of a Tafel plot, the straight line being obtained from a least squares fit:

$$\log(i_{\text{inh}}) = \frac{U}{131\,\text{mV}} - 6.806 \tag{28}$$

The potential dependence of the t^3-region is given by Equation 25: there is a slight dependence on b_{nucl} and a stronger one on b_{free}. The correlation between the slope b_3 of Fig. 6 and b_{nucl} and b_{free} is given by

$$\frac{1}{b_3} = \frac{\mathrm{d}\left(\log\left(\frac{\mathrm{d}i_{\text{pits}}}{\mathrm{d}t^3}\right)\right)}{\mathrm{d}U} = \frac{1}{b_{\text{nucl}}} + \frac{3}{b_{\text{free}}} \tag{29}$$

b_{nucl} is only positive, if $b_{\text{free}} > 3b_3$. From the slopes in Fig. 8 and Fig. 6 the following values can be taken: $b_{\text{free}} = 76$ mV and $b_3 = 21$ mV. This means $b_{\text{nucl}} \simeq 120$ mV, which corresponds to a simple transfer mechanism with $z = 1$. These values are used in the computations.

The overpotential of pit formation, $U - U_{\text{nucl}}$, is calculated using a value of $U_{\text{nucl}} = 400$ mV, which is the lower limit of desorption (Fig. 2). A numerical value of n' was obtained from a direct comparison of measured and calculated transients. The best fit was $n' = 7 \times 10^{11}\,\text{cm}^{-2}\,\text{s}^{-1}$. Values of n' can also be taken from an extrapolation of Fig. 6 to $U = 0$ V (Equation 25), but they are less precise.

Figure 9 shows calculated current transients according to Equation 24 for different potentials. Additionally, the calculated current transients at $U = 0.4$, 0.52 and 0.6 V are plotted together with the numbers of pits $n/10^{11}$ (Equation 18a), the radii r (Equation 15), and the total areas of all pits, Fig. 10. The radii vary from 1 nm in the beginning of the t^3-region of the transient to some 10 nm when the pits overlap and the current becomes constant. These

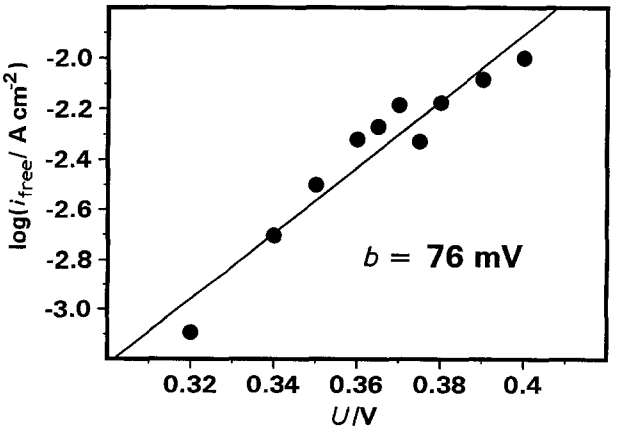

Fig. 7. Tafel plot of the corrosion current of a free copper surface in AHT·HCl solution, taken from potentiostatic transients. $c_{\text{inh}} = 2 \times 10^{-3}$ M, 0.5 M H_2SO_4.

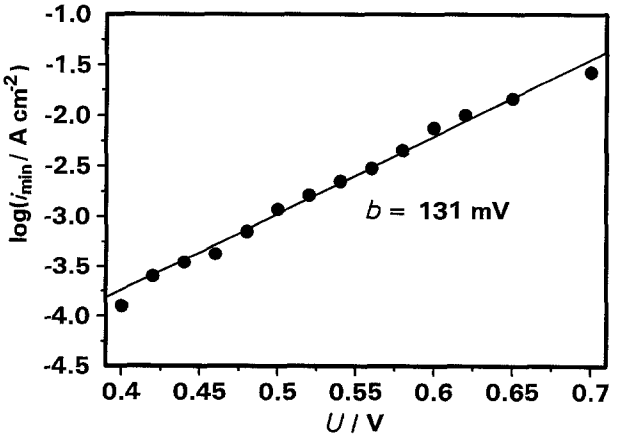

Fig. 8. Tafel plot of the corrosion current at the metastable inhibitor layer, values taken from Fig. 2.

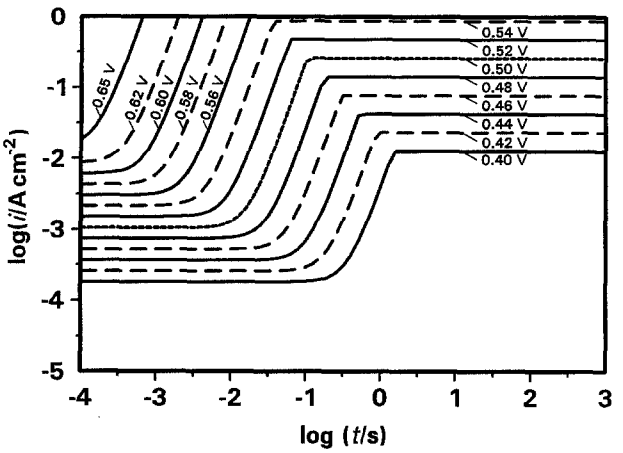

Fig. 9. Calculated current transients for the same potentials as in Fig. 2 according to Equations 22(b) and 23. Parameters of calculation: $U_{nucl} = 0.4\,V$, $n' = 7 \times 10^{11}\,cm^{-2}$, $b_{nucl} = 120\,mV$, $b_{free} = 76\,mV$.

values are very small and represent a lower limit of r, since the size of an AHT molecule is about 1 nm. This means that desorption of the AHT layer starts with an initial free surface with a size of approximately one molecule. The growth of a pit to its final size requires the desorption of about a hundred molecules.

The calculated radii $r(t)$ depend on i_{free}. The experimental values of i_{free} were taken from measurements at macroscopic surfaces. The corrosion current density of microscopic pits may be more than one decade higher due to their different diffusion geometry, [19].

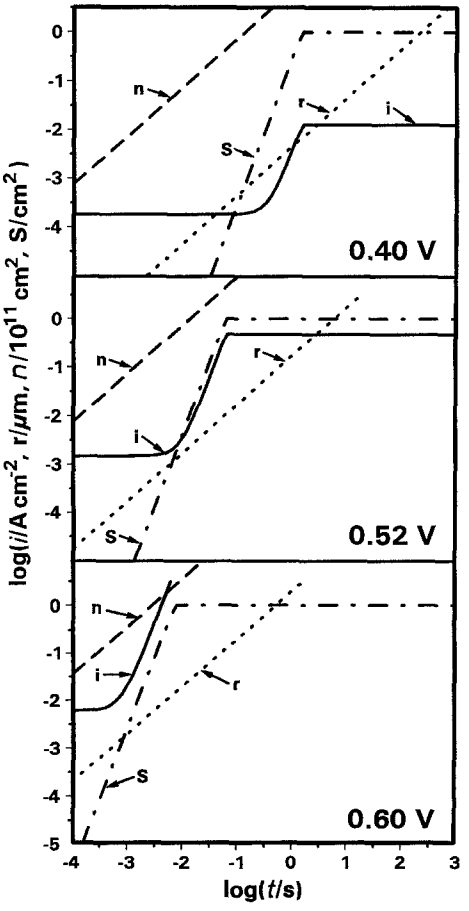

Fig. 10. Double logarithmic plot of the calculated current transients together with pit radii r, number of pits $n/10^{11}$, and total pit area S at $U = 0.4$, 0.52 and 0.6 V.

An increase of i_{free} yields a proportional increase of r and a corresponding decrease of n'. In agreement with this, a maximum radius of about 100 nm is also found in the investigations described in Section 4.3.2. Similar calculations were carried out considering a limited number of possible holes (Equation 22b), but the shape of the transients is very similar to those according to Equation 22(a). Therefore, the more complex Equation 22(b) was not used further.

Figure 11 compares experimental and calculated transients for the complete potential region. The fit is quite good, considering the following limitations of the model:

(i) The IR drop in the electrolyte for currents $i > 100\,mA\,cm^{-2}$ is not taken into account.
(ii) For potentials $U < 480\,mV$ a re-inhibition of pits is notable and reduces the experimental currents.
(iii) An overlapping of the pits in the final part of the transients is not included.

4.3. *Special transients*

The present interest was to design experiments with results predictable by the model. The t^3-dependence of the transient is determined by two effects: the formation rate of holes in the inhibitor layer and the geometrical shape of the pits. Both effects should be changeable independently. This was tested in two types of experiments which are presented as follows.

4.3.1. *Transients with a constant number of pits:* The formation of holes in the inhibitor layer increases exponentially with the potential. If the number of holes is already initially, the additional formation of holes at lower potentials is negligible and their total number remains almost constant. This is realized by a prepulse which is added in the beginning of the transient experiment. The prepulse must be high enough to form a sufficient number of small holes and short enough to prevent growth of the pits (typical values are 620 mV and 100 μs). At a lower potential the holes grown on without an increase in their number n. Hence, the slope of a prepulse

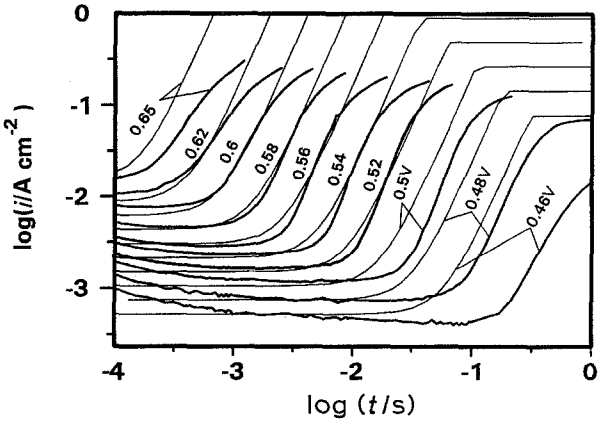

Fig. 11. Comparison of calculated current transients (thin lines) with the experimental ones from Fig. 2.

transient should be given by t^2, compared with t^3 of the standard transient (cf. Equation 25). Figure 12 shows such transients with or without a prepulse. Due to the logarithmic time scale the effects of the short prepulse on the current transient seem to be oversized.

The prepulse reduces the exponent of t approximately by 1, as expected, but a further decrease of the exponent with an increasing length of the prepulse is also observed. A prepulse of e.g. 200 μs causes an extremely high number of holes. Accordingly, the currents for $t < 3$ ms are increased by more than one decade. This means, using a ratio $i_{free}/i_{inh} = 100$, that more than 10% of the surface is covered with very small holes and, hence, their number is extremely high. An interaction between the holes (e.g. overlapping) becomes possible, which is not included in the model. The number of pits formed during a prepulse depends linearly on the pulse time t and exponentially the pulse potential. Experiments with different pre-pulses, where $t \exp(\eta/b_{nucl})$ was constant (Equations 18(a) and 23), should yield identical transients. From such measurements, a determination of b_{nucl} is possible. Unfortunately, the reproducibility was not sufficient to obtain a reliable value of b_{nucl}.

4.3.2. *Quasi two-dimensional electrodes:* In the experiments described earlier copper wire electrodes were used. The depth of the corrosion pits could increase up to some 100 μm. The idea was to use thin copper layers on a noble electrode (e.g. gold) as an electrode. In this case, the three-dimensional growth of the corrosion pits is reduced to two dimensions, when the radius of the pit reaches the thickness of the copper layer and, therefore, a significant bend in the transient should be observed.

Dense and homogeneous layers of copper with $d < 200$ nm were prepared on gold by electrodepostion. Transient measurements using these electrodes showed an additional bend at the end of the t^3-region. Hence, this experiment gives an estimate of the pit size. The radius of the oldest pits must be in the range of 100 nm. The pits are, in fact, very small and their number is, therefore, very high. A microscopical monitoring of the pit growth is almost impossible, because the pits are too small. A visual control becomes possible, when the current of the transients is constant and the mechanism described above is no longer valid. The structures seen in the microscope are not single pits due to the model but groups of overlapping pits with the resulting irregular shape. Hence, a further numerical analysis of the number of pits was unnecessary.

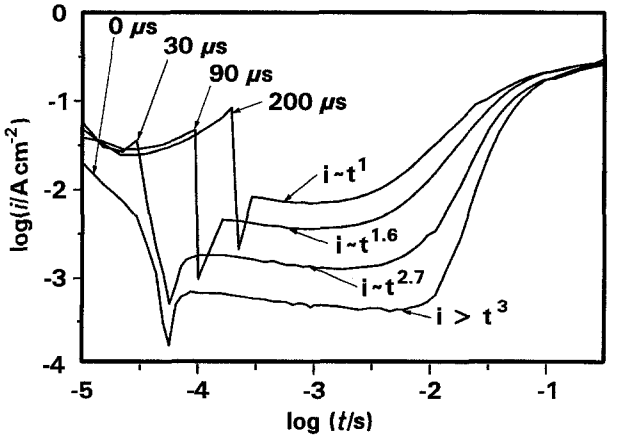

Fig. 12. Transients at $U = 0.52$ V with various pre-pulses (0.65 V and 0, 30, 90, and 200 μs). The prepulses seem to be oversized due to the logarithmic time scale.

4.4. *Conclusions*

The dissolution of inhibitor layers of AHT (3-amino-5-heptyl-1,2,4-triazole) on copper in 0.5 M H_2SO_4 was investigated by potentiostatic pulse measurements in a time range from 10 μs to 1000 s. The dissolution of this inhibitor is not accompanied by a notable charge transfer and, hence, the corrosion current of the uncovered parts of the copper electrode was taken to monitor this process. An analysis of the electrode capacity (Equation 7) gives the same results.

The potential dependent transients show three characteristic regions. Initially the inhibitor layer was found to be metastable and a small constant current of 'passive' corrosion with a b-factor of 131 mV (Equation 28) was observed. Holes of molecular dimensions are stochastically formed in the inhibitor layer with a constant formation rate $n' = 7 \times 10^{11}$ cm^{-2} s^{-1}. The nucleation rate is given by Equations 19(a) and 23 with $b_{nucl} = 120$ mV. The holes are the origins of an increasing number of growing hemispherical pits in the copper surface. Therefore, the total current, i, is dominated by the corrosion current and shows a t^3-dependence predicted by Equation 24. When the radii of the pits exceeds about 100 nm, most of the layer is dissolved, an increasing number of pits overlaps and i becomes constant. The electrode corrodes like a copper electrode in an inhibitor free solution ($b_{free} = 76$ mV). A visual monitoring of the pit growth during the t^3-period is not possible due to the small radii $r < 100$ nm of the holes. Therefore, the structures that were observable, are groups of overlapping pits with a resulting irregular shape. Tests with quasi two-dimensional electrodes prove that the pit radii are in the region of 100 nm at the end of the t^3-period.

The experimental transients were compared with calculated curves (Fig. 11). The fit was quite good considering the limitations of the model.

Acknowledgement

The financial support of this work by the Deutsche Forschungsgemeinschaft, Schwerpunktprogramm 'Elektrochemische Grundlagen der Korrosion', is gratefully acknowledged.

References

[1] K. Jüttner, W. J. Lorenz, W. Paatsch, M. Kendig and F. Mansfeld, *Werkst. u Korr.* **36** (1985) 120.
[2] B. E. Conway, *J. Electrochem. Soc.* **124** (1977) 410C.
[3] S. Gilman, *J. Phys. Chem.* **67** (1963) 78; *ibid.* **70** (1966) 2880.
[4] S. Trasatti and L. Formaro, *J. Electroanal. Chem.* **17** (1968) 343.
[5] D. M. Drazic, V. J. Drazic and V. Jevtic, *Electrochim. Acta* **34** (1989) 1251.
[6] M. M. Lohrengel, *in* 'Electrochemical and Optical Techniques for the Study and Monitoring of Metallic Corrosion', (edited by M. G. S. Ferreira, C. A. Melendres), Kluwer Academic Publishers, Fordrecht (1991) pp. 69–121.
[7] U. König, M. Beier and J. W. Schultze, *J. Electroanal. Chem.* **330** (1992), 615.
[8] M. Beier and J. W. Schultze, *Electrochim. Acta* **37** (1992), 2299.
[9] Henkel KGaA, Düsseldorf, Technical information sheet, Texamin AT (1986).
[10] J. W. Schultze, M. M. Lohrengel and D. Ross, *Electrochim. Acta* **28** (1983) 973.
[11] M. M. Lohrengel and D. Ebling, Dechema Monographs, Vol. 120, VCH Verlagsgesellschaft, Weinheim (1989) p. 213.
[12] Klaus Kluger, Diplomarbeit, Düsseldorf (1989).
[13] U. König and M. M. Lohrengel, Dechema Monographien, Band 102, VCH Verlagsgesellschaft, Weinheim (1986) p. 99.
[14] U. König, M. M. Lohrengel and J. W. Schultze, *Ber. Bunsenges. Phys. Chem.* **91** (1987) 426.
[15] M. Avrami, *J. Chem. Phys.* **7** (1939) 1103; *ibid.* **8** (1940) 212.
[16] H.-H., Strehblow, Habilitationsschrift, Freie Universatiät Berlin (1977).
[17] H.-J. Engell and N. D. Stolica, *Z. Phys. Chem.* **NF 20** (1959) 113.
[18] J. W. Schultze, *Ber. Bunsenges. Phys. Chem.* **74** (1970) 705.
[19] R. M. Wightman and D. O. Wipf, 'Electroanalytical Chemistry', Vol. 15, (ed. A. Bard), Marcel Dekker, New York and Basel (1989).